Bioactive Materials 14 (2022) 206–218

Contents lists available at ScienceDirect

Bioactive Materials

journal homepage: www.keaipublishing.com/en/journals/bioactive-materials

Promotion of right ventricular outflow tract reconstruction using a novel cardiac patch incorporated with hypoxia-pretreated urine-derived stem cells

Long-Mei Zhao [a,1], Long Wang [b,c,1], Wen-Qian Zhang [a], Rui Wang [a], Xiu-Zhen Zhang [a], Xiong-Xin Lei [a], Yan Liang [d], Yu-Ting Song [a], Qing-Yi Zhang [a], Ke Lin [b,**], Hui-Qi Xie [a,*]

[a] Laboratory of Stem Cell and Tissue Engineering, Orthopedic Research Institute, Med-X Center for Materials, State Key Laboratory of Biotherapy, West China Hospital, Sichuan University, Chengdu, Sichuan, 610041, China
[b] Department of Cardiovascular Surgery, West China Hospital, Sichuan University, Chengdu, Sichuan, 610041, China
[c] Department of Cardiovascular Surgery, Shandong Provincial Hospital, Shandong First Medical University, Jinan, Shandong, 250021, China
[d] Research Core Facility, West China Hospital, Sichuan University, Chengdu, Sichuan, 610041, China

ARTICLE INFO

Keywords:
Congenital heart disease
Polypyrrole
Polyurethane/small intestinal submucosa
Hypoxia
Urine-derived stem cells

ABSTRACT

Approximately 25% of patients with congenital heart disease require implantation of patches to repair. However, most of the currently available patches are made of inert materials with unmatched electrical conductivity and mechanical properties, which may lead to an increased risk for arrhythmia and heart failure. In this study, we have developed a novel Polyurethane/Small intestinal submucosa patch (PSP) with mechanical and electrical properties similar to those of the native myocardial tissue, and assessed its feasibility for the reconstruction of right ventricular outflow tract. A right ventricular outflow tract reconstruction model was constructed in 40 rabbits. Compared with commercially available bovine pericardium patch, the PSP patch has shown better histocompatibility and biodegradability, in addition with significantly improved cardiac function. To tackle the significant fibrosis and relatively poor vascularization during tissue remodeling, we have further developed a bioactive patch by incorporating the PSP composites with urine-derived stem cells (USCs) which were pretreated with hypoxia. The results showed that the hypoxia-pretreated bioactive patch could significantly inhibit fibrosis and promote vascularization and muscularization, resulting in better right heart function. Our findings suggested that the PSP patch combined with hypoxia-pretreated USCs may provide a better strategy for the treatment of congenital heart disease.

1. Introduction

Congenital heart diseases (CHD) are relatively common and can manifest as anatomical and/or functional abnormalities of the cardiovascular system. The prevalence of CHDs among newborns is September 6, 1000 in North America, February 8, 1000 in Europe, and March 9, 1000 in Asia [1,2]. Approximately 25% of CHD patients will require implantation of a cardiac patch to repair their defect during the first year of life, and the selection of patch is crucial for the restoration of cardiac function [3]. Currently available commercial patches include biological and synthetic materials such as knitted polyethylene terephthalate, expanded polytetrafluoroethylene, glutaraldehyde-fixed bovine pericardium, etc. [4–7] The electrical conductivity and mechanical properties of such materials do not match with those of normal myocardium, which may lead to an increased risk for arrhythmia, heart failure, and even sudden cardiac death [8–12]. For pediatric patients, the lack of growth potential of such patches is also an important issue. Approximately 14% of children may require re-operation to replace their patches [13]. A new type of material with conductivity, biodegradability and mechanical properties is therefore in great demand.

Peer review under responsibility of KeAi Communications Co., Ltd.

* Corresponding author. Laboratory of Stem Cell and Tissue Engineering, Orthopedic Research Institute, Med-X Center for Materials, State Key Laboratory of Biotherapy, West China Hospital, Sichuan University, 1 Keyuan Fourth Road, Gaopeng Avenue, Chengdu, Sichuan, 610041, China.
** Corresponding author. Department of Cardiovascular Surgery, West China Hospital, Sichuan University, 37 Guoxuexiang, Chengdu, Sichuan, 610041, China.
E-mail addresses: edidian@163.com (K. Lin), xiehuiqi@scu.edu.cn (H.-Q. Xie).
[1] These authors have contributed equally to this work.

https://doi.org/10.1016/j.bioactmat.2021.11.021
Received 6 September 2021; Received in revised form 2 November 2021; Accepted 15 November 2021
Available online 30 November 2021

The majority of cardiac tissue engineering researches have focused on the repair of myocardial infarction [3,14,15], whilst only a few have devoted to the development of cardiac patches [16–18]. Indeed, most of such studies have focused on the physicochemical and biological properties of the patches, but have not investigated their feasibility for repairing the cardiac defects *in situ*. In this study, we have developed a cardiac patch purported for ventricular outflow tract reconstruction and validated its effect for the repair of right ventricular outflow tract (RVOT).

Polyurethane/Small intestinal submucosa (PU/SIS) is a chemically crosslinked scaffold derived by incorporating polyurethane into small intestinal submucosa. The PU/SIS composites have retained the ability of polymers for regulating their degradation rate and mechanical properties whilst promoting cell adhesion and proliferation. Our previous study has shown that the PU/SIS composites possessed a high bioactivity and resilience, and could be used for soft tissue engineering. Meanwhile, the mechanical properties of the PU/SIS composites are similar to those of myocardial tissue [19,20], suggesting that it has a potential to be developed as a cardiac patch.

As one of the most stable conductive polymers, polypyrrole (PPy) has attracted much attention in recent years for its easy synthesis, high electrical conductivity [21], good biocompatibility [22], and antibacterial activity [23]. A number of studies have shown that the PPy may be used as scaffold for nerve [24], muscle [25], and bone growth [26, 27] and as a substrate for electrically stimulated cell growth [25]. In addition, PPy-containing conductive complexes have been used for the treatment of myocardial infarction and have shown be effective for preventing arrhythmia, promoting revascularization, and inhibiting myocardial remodeling [18,28,29]. On the other hand, however, the PPy is weak, brittle, and rigid, which has hindered its application in biomedicine [27]. To incorporate PPy with other materials with better mechanical properties may overcome the above problems. In this study, we have combined the PU/SIS with the PPy to produce a PSP complex with high resilience and electrical conductivity, and investigated its feasibility for the reconstruction of RVOT.

Human mesenchymal stem cells (MSCs) have been considered as a promising cell source for cardiac repair. Studies have elucidated the role of the MSCs in the recovery of cardiac functions in myocardial infarction, including enhancement of neovascularization and reducing pathological fibrosis associated with upregulated expression of genes implicated in cardiac repair [30,31]. As a more recently discovered type of adult MSCs, urine-derived stem cells (USCs) can be isolated through a simple, non-invasive, and low-cost approach, which can create personalized grafts for tissue regeneration [32]. Studies have proven that the USCs can respond promptly to environmental signals to modulate their secretory activities [33]. Appropriate preconditioning may induce the MSCs to release secretomes with enhanced regenerative potential [34, 35]. Hypoxic preconditioning can induce angiogenesis via hypoxia inducible factor-1α (HIF-1α) and vascular endothelial growth factor (VEGF).

In this study, we have developed a novel cardiac patch with high resilience, excellent electrical conductivity, good biocompatibility and biodegradability by coating the PU/SIS with the PPy, and assessed its physicochemical, mechanical, and electrical properties. Furthermore, we have also constructed a PSP + USCs bioactive cardiac patch and evaluated the effect of hypoxic preconditioning of the patch for the reconstruction of ventricular outflow tract.

2. Materials and methods

2.1. Preparation of the PSP composites

The PSP composites were prepared by using an *in situ* polymerization method. In brief, PU/SIS sponges were prepared with a previously described method (details are provided in the supplement) [20]. Thereafter, the PU/SIS sponge (3 × 3 × 0.3 cm3) was immersed in 0.3 mL pyrrole monomer solution (0.4 mol/L) for 30 min to ensure uniform penetration of the PPy monomer into the scaffold. Next, the PU/SIS scaffold was soaked in a FeCl3 solution (1 mol/L) at room temperature for 4 h to allow the PPy to polymerize. The PSP composites were then taken out, cleaned with water until the rinsing solution became clear, and subjected to vacuum freeze-drying overnight.

2.2. Physicochemical characterization

2.2.1. Attenuated total reflectance-Fourier transformed infrared (ATR-FTIR) spectroscopy

The ATR-FTIR spectra were measured using a Nicolet 6700 FTIR spectrometer over the wavelength range of 4000–400 cm–1.

2.2.2. Determination of the mechanical property

Mechanical property of the PSP composites was determined with an Instron 5567 Instrument (Instron Corporation). All samples (75 × 4 × 2 mm3) were equilibrated in phosphate buffer solution for approximately 30 min prior to the testing. Tensile test was conducted at a speed of 100 mm/min. The stress-strain curves were recorded until failure of the sample, with which the tensile modulus was calculated.

2.2.3. Scanning electron microscopy

The surface of the PSP composites was characterized under a scanning electron microscope (SEM) (EVO 10, ZEISS) at an accelerating voltage of 15 kV. The freeze-dried samples were coated with Au and observed under SEM at a magnification power of 100.

2.2.4. Atomic force microscopy

The roughness characterization of the PSP composites was determined using an atomic force microscope (AFM) (Smart SPM, AIST-NT). AFM image scans of 1 mm^2 were conducted in air using AC mode image. The roughness value (Rms) for each film was calculated from the AFM images.

2.2.5. Water contact angle

The hydrophilicity of the PSP composites was characterized by static water contact angle (WCA), which was measured with a contact angle goniometer (OCA 15/20, Future Digital Scientific Corp.) with 2 μL water as the probe liquid. At least three measurements were taken for each sample.

2.2.6. Electrical conductivity assay

The electrical conductivity of the PSP composites was measured by using a conventional four-point probe method (MCP-T700, Mitsubishi), where two pairs of contacts were used to measure the conductivity. The samples were cut into 15 mm × 15 mm pieces, and 10 detection points were randomly selected for calculating the average electrical conductivity.

2.3. Isolation and characterization of human USCs

The USCs were isolated from urine samples from healthy male adult donors (20–30 years old) by using a previously described method [32]. Briefly, fresh urine was collected and centrifuged for 10 min at 1500 rpm. The sediment was washed twice in PBS. The cells obtained were cultured in USCs medium, and P3 USCs were used for subsequent experiments. Cultured USCs were subjected to flow cytometry analysis for their potential for osteogenic and adipogenic differentiation (detailed procedures are described in the Supplement).

2.4. Biocompatibility

2.4.1. Cytocompatibility assay

The effect of the PSP composites on cell proliferation was evaluated with a CCK-8 assay (DOJINDO, Japan) by following the manufacturer's

protocol. Briefly, the extract solution was prepared by soaking the materials in an USCs medium (area: volume = 1 : 6) at 37 °C for 24 h. Meanwhile, the USCs were seeded on a 96-well plate at a density of 5×10^4 cells/well and cultured with the medium. After 24 h of culture, the medium was replaced with extract solution. Their viability was tested using a CCK-8 assay kit on days 1, 3, 5, and 7. Bovine pericardium (Synovis Surgical Innovations Inc, USA), a commercially made cardiac patch, was used as the control. Viability of the cells on the PSP composites was evaluated with a Calcein-AM/PI Double Stain Kit (Yeasen, China). In brief, the P3 USCs were seeded onto the PSP composites at a density of 2×10^4 USCs/cm^2. Cell/scaffold constructs were incubated in sterile PBS containing 2 mM Calcein-AM and 4 mM ethidium homodimer-1 for 20 min at 37 °C in the darkness after 1, 3 and 5 days of culture. The samples were then observed under a confocal microscope (Nikon A1RMP+, Nikon Instruments Inc., Tokyo, Japan).

2.4.2. Histocompatibility assay

Hemolysis test was performed according to the ISO standard 10993:2018. Briefly, fresh venous blood sampled from healthy adult New Zealand white rabbits was diluted to remove external and lysed red blood cells (RBCs). The sample was then diluted with PBS to obtain a RBC suspension. The PSP and bovine pericardium were added into the suspension (300 μL) and incubated at 37 °C for 60 min. Normal saline and distilled water were respectively used as positive and negative controls. After the incubation, the samples were centrifuged. Optical density (OD) of the supernatant was measured under a wavelength of 545 nm.

Histocompatibility and degradation rate of the PSP composites were investigated *in vivo* through subcutaneous implantation experiments. Two separate skin incisions were made on the back of Sprague-Dawley (SD) rats (n = 12). The PSP composites and bovine pericardium (control) were carefully implanted into subcutaneous pockets. The animals were sacrificed at 4, 8, and 12 weeks after the surgery. The implants and surrounding tissues were collected and fixed with 4% paraformaldehyde for histological evaluation. Degradation rates of the PSP composites and bovine pericardium were calculated based on their auto-fluorescence at 488 nm.

2.5. Preparation of the USCs + PSP composites

Prior to cell seeding, the PSP composites were immersed in USCs medium for 24 h. The USCs were then seeded onto the surface of each PSP composite at a density of 3×10^4 cells/cm^2. The PSP + USCs composites were divided into the PSP + USCs (N) group, which was cultured in a normoxic environment (21% O_2, 5% CO_2), and the PSP + USCs (H) group, which was cultured in a hypoxic environment (1% O_2, 5% CO_2).

2.6. Real-time polymerase chain reaction (RT-PCR)

After 24 h of incubation, total RNA was extracted from the cultured cell-scaffold complex using Trizol reagent (Life Technologies, USA), and cDNA was synthesized by using a PrimeScript™ RT reagent Kit (Takara, Japan). RT-PCR was carried out in a SYBR Green PCR master mix (Takara, Japan) on a Lightcycler 96 system (Roche, Switzerland). The primers for RT-PCR are listed in Table S1. Relative level of gene expression was expressed as $2^{-\Delta\Delta Cq}$.

2.7. Enzyme-linked immunosorbent assay (ELISA)

After 24 h of incubation, supernatant was collected from the cultured cell-scaffold complex and centrifuged at 1000 g for 5 min to remove the cell debris. Epithelial growth factor (EGF), vascular endothelial growth factor (VEGF) and basic fibroblast growth factor (bFGF) were measured by using an ELISA kit (Ray biotech, USA) by following the manufacturers' instruction.

2.8. Construction of a ROVT model

All studies involving animal experiments have been approved by the Institutional Animal Care and Use Committee of Sichuan University (No. 2019161A). The surgical protocol was described by Pok et al. [36] Forty-three male New Zealand white rabbits were randomly assigned to 4-week bovine pericardium group (n = 3), 4-week PSP group (n = 3), 4-week PSP + USCs(N) group (n = 3), 4-week PSP + USCs(H) group (n = 3), 8-week bovine pericardium group (n = 5), 8-week PSP group (n = 3), 8-week PSP + USCs(N) group (n = 3), 8-week PSP + USCs(H) group (n = 3), 12-week bovine pericardium group (n = 4), 12-week PSP group (n = 5), 12-week PSP + USCs(N) group (n = 4) and 12-week PSP + USCs (H) group (n = 4). All animals were abdicated for food and drink for 6 h before the surgery. New Zealand white rabbits weighted 2–3 kg were anesthetized with 3% pentobarbital sodium (2 mL/kg), endotracheally intubated, and mechanically ventilated with an animal ventilator, with the exhalation: inhalation ratio of 5 : 4, tidal volume of 35 mL, and a breathing rate of 30 times/min. Left thoracotomy and pericardiotomy were used to expose the heart. An 8 mm diameter purse was placed in the wall of RVOT with a 7-0 suture and constricted with a 22G vascular cannula to prevent bleeding (Fig. 5A). Approximately 3/4 of the bulge was partially excised to form a 6 mm full-length defect. The tourniquet was briefly released to verify the patency of the artificial defect in the RVOT. A patch of approximately 7 mm in diameter was sutured along the edge of purse-string suture to cover the defect of the right ventricle by continuous suturing. Finally, the chest cavity, muscles and skin were sutured in 3 layers. Post-surgery intramuscular penicillin (100,000 U/day) was administered for 7 days to prevent infection.

2.9. Magnetic resonance imaging

All animals underwent magnetic resonance imaging (MRI) scans 12 weeks after the surgery for the measurement of cardiac function. The animals were anesthetized and endotracheally intubated. Metoprolol solvent was slowly pushed via intravenous access until the heart rate has dropped below 180/min. The animal was then placed into the coil for positional scanning. All scans were performed using a Siemens Skyra 3.0 T magnetic resonance scanner with cardiac electrode pads attached to the chest. Scan sequences were triggered by electrocardiography (ECG) during end-expiratory pauses by using a ventilator. Cardiac MRI was performed using a steady-state free motion (SSFP) sequence. The parameters of the right ventricle scan were: TR 51.22 ms, TE 1.70 ms, flip angle 15°, layer thickness 3 mm, layer spacing 50%, the field of view 213 mm × 171.16 mm. All images were analyzed with a workstation. Right ventricular end-diastolic volumes (RV-EDV) and end-systole volumes (RV-ESV) were recorded. The right ventricular ejection fraction (RVEF) was calculated with *Eq.* [1].

$$RVEF = \frac{EDV - ESV}{EDV} \times 100\% \quad (1)$$

2.10. Histology and immunofluorescence staining

The animals were euthanized at 4, 8, and 12 weeks postoperatively, and photographs were taken to record the gross morphology of the hearts. The samples were frozen in OTC compound (Solarbio, China) and cut into 5 μm-thick sections with a cryostat (Leica, Germany). The sections were subjected to Hematoxylin and Eosin (H&E) staining to observe tissue regeneration and scaffold degradation. Patch-induced fibrosis was assessed with Masson's trichrome staining. Furthermore, specimen of kidney, lung, and liver were taken at 12th week, rinsed with 0.9% NaCl to remove the blood, fixed with 10% formalin overnight, dehydrated through an alcohol gradient, and embedded in paraffin. Sections were cut at 3–5 μm in thickness and subjected to H&E staining.

For immunofluorescence staining, the sections were fixed in 10% formaldehyde for 10 min, blocked with 10% goat serum (Beyotime,

C0265) at 37 °C for 30 min, and incubated at 4 °C with specific anti-α-smooth muscle actin antibody (α -SMA; 1 : 200, Abcam, ab7817), anti-Cardiac Troponin I antibody (1 : 200, Abcam, ab56357) and anti-CD31 antibody (1 : 100, Abcam, ab182981) overnight. Subsequently, the sections were treated with goat anti-mouse secondary antibody (1 : 500, Jackson ImmunoResearch, 115-605-003), goat anti-rabbit secondary antibody (1 : 500, Jackson ImmunoResearch, 111-605-003) or donkey anti-goat secondary antibody (1:200, Abcam, ab6566) at 37 °C for 1 h. Nuclei were counter-stained with 4,6-diamidino-2-phenylindole (DAPI, Invitrogen, P36931) for 5 min at room temperature. Fluorescence images were taken under a Zeiss 2.1 microscope and evaluated with Image J software.

2.11. Flame atomic absorption spectrometry

Calcium content was measured with flame atomic absorption spectrometry. Briefly, four pieces of tissues from the regenerative area were removed and dried for 48 h at 50 °C at 12 weeks postoperatively. The samples were weighed and dissolved in 1 mL HNO_3 and 0.5 mL $HClO_4$. Subsequently, the samples were washed 3 times with 0.3 mL deionized water, and the rinsing solution was collected. After adding 40 μL of 0.5% $LaCl_3$ to the washing solution, the calcium content was measured at 422.7 nm with an Analyst 400 (PerkinElmer Life and Analytical Sciences, USA) instrument.

2.12. Statistical analysis

All results were presented as mean ± standard deviation. Statistical analysis was carried out by the independent-samples *t*-test or one-way analysis of variance (ANOVA) using GraphPad Prism 8 software. Comparison of three or more groups was made with one-way ANOVA. $P < 0.05$ was considered to be statistically significant.

3. Results

3.1. Preparation and characterization of the PSP composites

In this study, we have compounded the PU/SIS with PPy to prepare a highly elastic conductive PSP complex. The principle and procedure for the preparation are shown in Fig. 1. After polymerization by pyrrole monomers, the surface of PU/SIS sponges has changed from white to black (Fig. 2A).

ATR-FTIR spectra of the PU/SIS and PSP were recorded with an FTIR spectrometer (Fig. 2B). For PU/SIS, the peaks at 1670 cm^{-1} and 1531 cm^{-1} were assigned to the C═O vibration stretching and N–H angular deformations, along with the band at 1241 cm^{-1} resulted from C–O–C stretching of the PU/SIS. For PSP, the bands at 3500 cm^{-1} to 3300 cm^{-1} may be attributed to the N–H stretching vibration, and the broader band may be due to the formation of hydrogen bonds between the PPy and PU/SIS. In addition, a characteristic peak of PPy was noted in the PSP spectra. The bands at 1533 cm^{-1} and 1365 cm^{-1} are associated with the vibration of C–C stretching in the aromatic rings, along with the peak at 1108 cm^{-1} and 933 cm^{-1}, which may be attributed to the C–H and N–H bend vibration of the doped PPy chain. Above results have confirmed the presence of PPy in the PSP composites.

As the pump of the circular system, the heart undertakes a great burden for work. Patches applied for heart repair will require good mechanical property similar to those of the native cardiac tissues. A patch with too high or too low elastic tensile modulus may result in cardiac dysfunction. In this study, the tensile modulus of the PSP patch was measured. As shown in Figs. 2C and S2E, the elastic modulus of the PSP was 211 ± 9.77 KPa, which was similar to that of myocardial tissue (20–500 kPa) [19], thereby can meet the requirement of myocardial contraction. Besides, surface modification of the PPy has not affected the mechanical properties of the PU/SIS, with the elastic modulus of the PSP showing no significant difference from that of the PU/SIS.

The myocardium can transmit electrical impulses through intercellular gap junctions to enable its synchronous contraction. Non-conductive cardiac patches may result in asynchronous contraction of

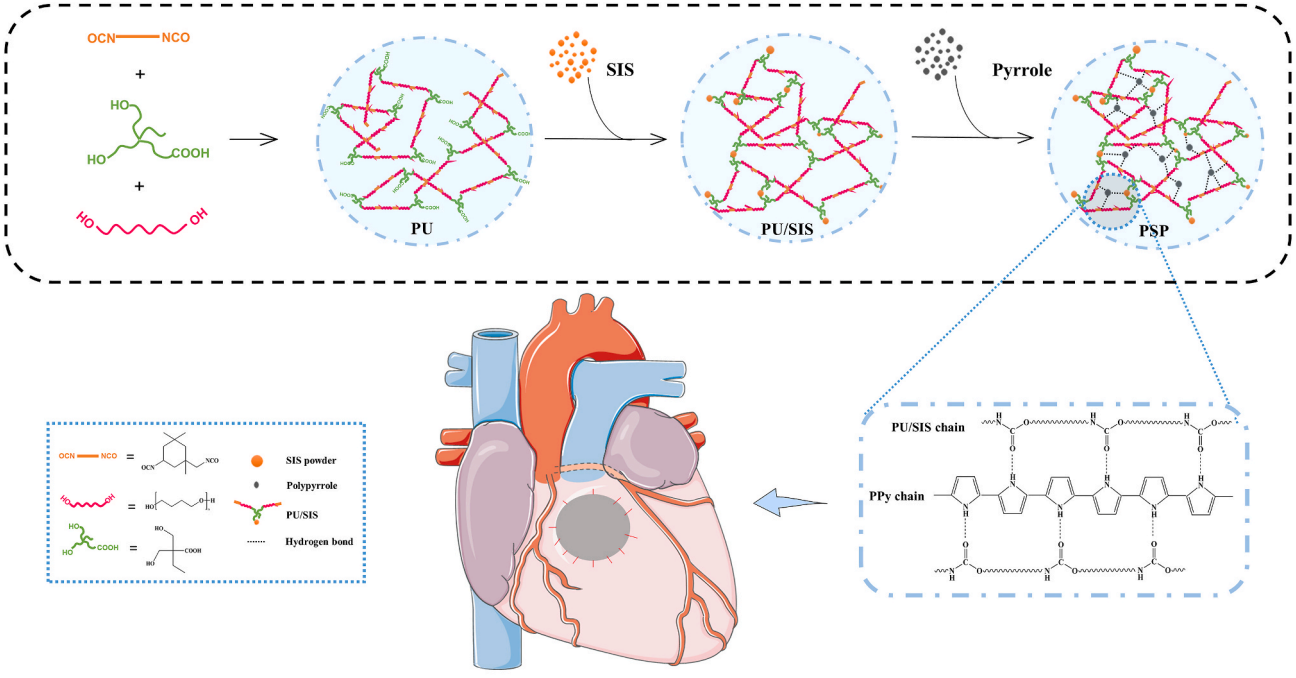

Fig. 1. Schematic illustration for the preparation of the PSP composite and its application in a rabbit model for right ventricle wall replacement.

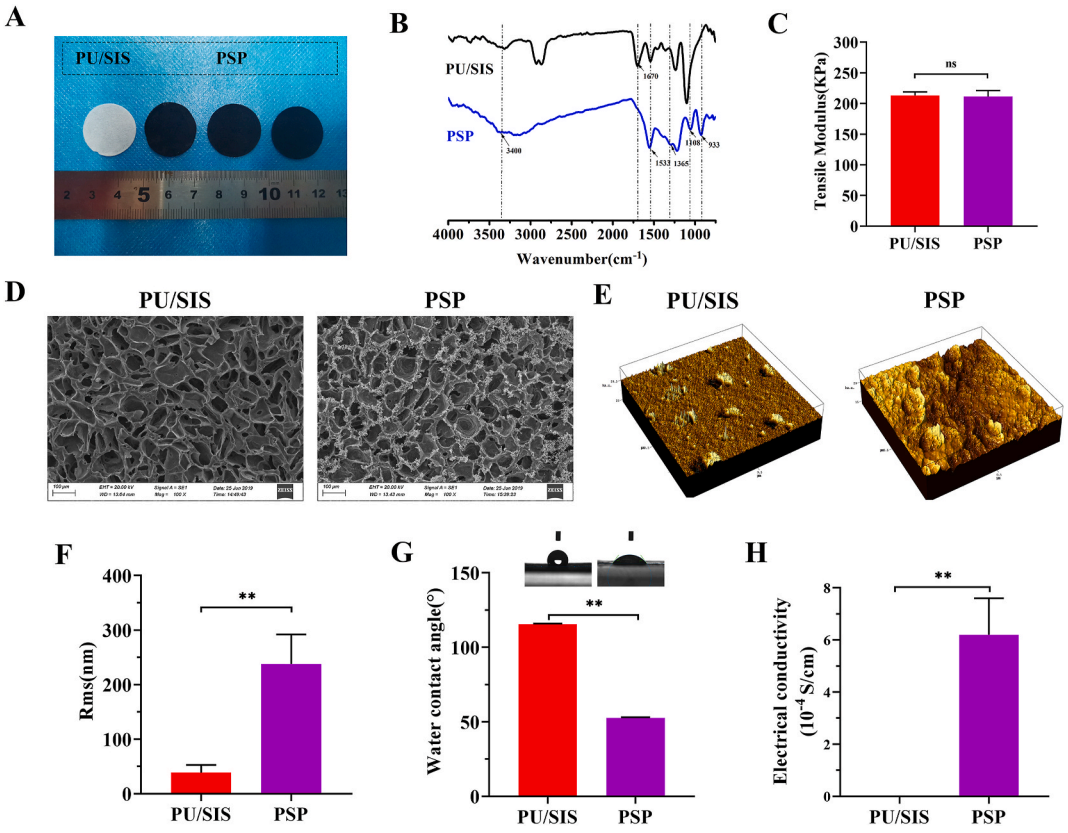

Fig. 2. Physicochemical and morphological properties of the PSP composites. (A) Gross appearance. (B) FTIR spectra of the PU/SIS and PSP composites. (C) Tensile modulus of the PU/SIS and PSP composites. (D) Ultrastructure of the PU/SIS and PSP composites under a SEM. (E, F) Surface morphology and roughness characterized by AFM. (G) Hydrophilicity of the PU/SIS and PSP composites as assessed with water contact angle. (H) Electrical conductivity measured with a four-point probe method. Data are represented by mean ± SD. $^{*}P < 0.05$, $^{**}P < 0.01$ by *t*-test.

the native cardiac tissue and cardiac patch, for they cannot transmit electrical impulses efficiently. As shown in Fig. 2H, a four-point probe measurement has suggested that the PU/SIS was non-conductive. By contrast, the PSP composites possessed excellent conductivity similar to that of native myocardium (0.0016 S/cm to 5 × 10^{-5} S/cm) [17,37].

SEM and AFM were used to detect the surface topology of the PU/SIS and PSP composites (Fig. 2D and E). The surface of the PU/SIS scaffold exhibited interconnected and smooth pores. Cross-sectional SEM images of the PSP showed that the PPy has distributed uniformly within the PU/SIS scaffold, generating a rough surface. At high magnification, the PPy was visible as nanoparticles attached to the surface of the PU/SIS scaffold (Fig. S1). AFM showed that the PU/SIS surface was uniform and smooth, while larger nodules have appeared on the PSP surface. Compared with the PSP, the roughness (Rms) of the PU/SIS was lower (Fig. 2F).

As an important feature of surface properties, hydrophilicity has a significant impact on the biocompatibility of the scaffold. In this study, hydrophilicity was valued with the water contact angle. The lower the water contact angle, the better the hydrophilicity of the scaffold. As shown in Fig. 2G, the water contact angle of the PU/SIS was significantly greater than that of the PSP composites ($P < 0.01$), which proved that the *in situ* polymerized PPy has significantly increased the hydrophilicity of the scaffolds. We speculate that the reduced water contact angle of the PSP might be due to the formation of hydrogen bonds between the PU/SIS and PPy, in addition to the introduction of a large number of hydrophilic pyrrole groups into the scaffold. Above results implied that the PSP composites might have better biocompatibility compared with the PU/SIS composites, which are beneficial to cell adhesion, proliferation, and migration.

3.2. Biocompatibility and biodegradability of the PSP patch

The USCs were extracted and validated as previously described [32]. As shown in Fig. S3A, the USCs isolated from fresh urine samples have formed colonies within 7 days. The isolated USCs could undergo osteogenic and adipogenic differentiation in vitro, and were positive for CD29, CD73, CD105, and CD90, but negative for CD34, CD45, and HLA-DR (Figs. S3B and S3C).

To assess the cytocompatibility of the PSP patch, a CCK-8 assay was carried out with commercially made bovine pericardium as the control. As shown in Fig. 3A, the PSP patch has exhibited no cytotoxicity. No significant difference was detected in the proliferation rate between the PSP patch and bovine pericardium. By Live/Dead staining, no obviously dead cells were found in either of them (Fig. 3B). The USCs have grown uniformly on the surface of bovine pericardium, whilst aggregated and grown into the pores of PSP patches. By hemolytic testing, the hemolysis rate of the PSP patch was less than 5% (Fig. 3C), which indicated sound hemocompatibility. Furthermore, the PSP patch has exhibited better histocompatibility compared with the bovine pericardium. As shown in Fig. 3D, a large number of cells have aggregated in the middle of the PSP composites, whereas virtually no cell infiltration was noted with the bovine pericardium patch.

Biodegradability of cardiac patches is critical to the outcome of long-term repair. Non-degradable cardiac patches can often lead to graft thickening, which may increase the risk of immunogenicity and disease transmission. As shown in Fig. S4, there was no significant difference in the degradation rates of bovine pericardium and PSP patches in vitro material degradation experiments conducted at 37 °C in PBS and the oxidative (3% H_2O_2) media for 60 days. In this study, we have assessed *in vivo* degradation of the PSP patch and bovine pericardial patches by

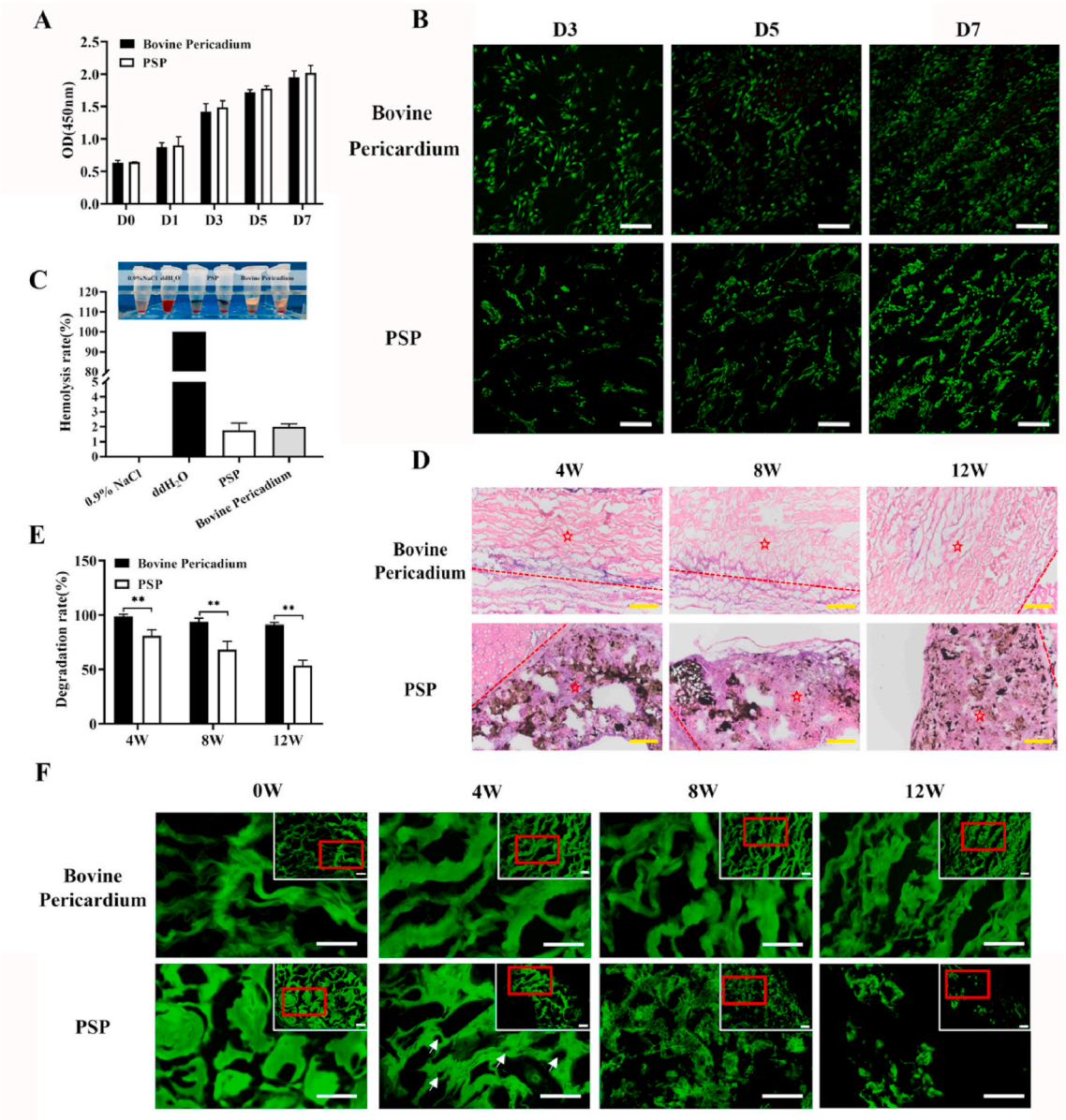

Fig. 3. Biocompatibility of the PSP composites. (A) Viability of the USCs as estimated by a CCK-8 assay after 1, 3, 5, and 7 days of incubation in the PSP and bovine pericardium extracts. (B) Viability of the cell on various materials as assessed by Calcein-AM/PI staining. Scale bars = 100 μm. (C) Hemocompatibility of the PSP patches. (D) Subcutaneous implantation of the bovine pericardium and PSP patches at 4, 8, and 12 weeks postoperatively. Dotted line indicated the border between scaffold and native tissue. ☆Indicates patches. The black parts represent PSP patches. Scale bar = 200 μm. (E) Analysis of the degradation rate *in vivo* at various time points. Data are represented by mean ± SD. $^{*}P < 0.05$, $^{**}P < 0.01$, one-way ANOVA. (F) The degradation of PSP composites and bovine pericardium. White arrows indicated the holes in PSP patch due to degradation. Green fluorescence represents the patches. Scale bar = 50 μm. (For interpretation of the references to color in this figure legend, the reader is referred to the Web version of this article.)

determining their autofluorescence intensity at 488 nm (Fig. 3E & F). Fluorescence is closely related to the chemical structure of the material itself. Fluorescence-producing conjugate structures are present in both PSP and bovine pericardium. Damage to the chemical structure may results in decay of fluorescence intensity. The results indicated that the PSP patches have good biodegradability (Fig. 3F). The original skeletal structures of both the PSP and bovine pericardium patches were continuous and intact. At 4 weeks postoperatively, partial degradation began in the middle of the PSP scaffold and there were many small holes in the middle of the PSP patch due to degradation. At 8 weeks postoperatively, the PSP patch further began to degrade and its surface took on a honeycomb form. At 12 weeks postoperatively, the integrity of PSP has broken down while the bovine pericardium was hardly degraded. Above results suggested that the PSP patch had better histocompatibility and biodegradability compared with commercially made bovine pericardial patches.

3.3. *Hypoxic treatment promoted the expression and secretion of angiogenic-associated cytokines by the PSP + USCs composites*

Microenvironment may significantly influence the proliferation and differentiation of stem cells, and hypoxia is one of the key features of the stem cell niche. Hypoxic pretreatment can enhance adaptation of the stem cells to the ischemic tissue microenvironment and their ability to repair. In this study, the USCs were cocultured with the PSP for the construction of the PSP + USCs bioactive cardiac patch, and the effect of hypoxic pretreatment on the paracrine activity of the PSP + USCs composites was investigated. After 24 h of hypoxic pretreatment, the

USCs have exhibited good activity (Fig. 4A). Expression of stemness and angiogenesis-related genes of the USCs, including NANOG, SOX-2, OCT-4, VEGF, bFGF, and EGF, was determined with RT-PCR. The results showed that the hypoxic pretreatment did not affect the expression of stemness factors (Fig. 4B), but enhanced the expression of angiogenesis-related genes (VEGF, bFGF, and EGF) in the PSP + USCs(H) group (Fig. 4C). ELISA assay also confirmed that the PSP + USCs(H) group has secreted more angiogenesis-related growth factors (VEGF, bFGF, and EGF) compared with the PSP + USCs (N) group (Fig. 4D).

3.4. Reconstruction of the RVOT with the PSP composites used as cardiac patch in an animal model

To assess the feasibility of the PSP patches for the repair of cardiac defect, a RVOT reconstruction model was established. The detailed surgical procedure was shown in Fig. 5A. Two animal in the 8-week pericardium group died from infection at 4 weeks postoperatively and one animal in the 12-week PSP group died from cardiac arrest the second day post-surgery. All of the 40 animals have survived to the endpoint and were included in the statistical analysis. Fig. 5B has provided a gross view for the patched hearts in each group at various time points. The PSP patches had a dark appearance, whilst the bovine pericardium had a yellowish appearance on the patched area. All patches have provided surgical operation with adequate strength of suture fixation, no bleeding through the patch area and a rough surface without any tissue coverage (Fig. S5). At 4 weeks after the operation, the edges of all patches have integrated with the native tissue. Compared with the PSP group, there was significantly less patches bared outside and more tissues regeneration in the PSP + USCs (H) groups at 8 weeks postoperatively, suggesting that the hypoxic-pretreated USCs have provided a better regenerative microenvironment for tissue repair (Fig. 5C). At 12 weeks postoperatively, the surfaces of the patches in all groups were covered with new tissue and almost no patches were exposed.

Followed-up MRI was used to monitor cardiac remodeling and recovery of the cardiac function at 12 weeks postoperatively (Fig. 5D). Right ventricular end-diastolic volumes (RV-EDV), end-systole volumes (RV-ESV) and right ventricular ejection fraction (RVEF) were recorded to qualify the cardiac function (Fig. 5E). No sample has displayed RVOT obstruction by MRI analysis. The RVEF of the PSP group was significantly improved compared with the bovine pericardium group ($P < 0.05$), but was not significantly different from the PSP + USCs (N) group ($P > 0.05$). The RVEF of the PSP + USCs (H) group was higher than those of other groups ($P < 0.01$).

3.5. Suppression of fibrosis by the hypoxia-pretreated bioactive patches

Pathological changes and degradation of the scaffold in the right ventricle wall during the period of regeneration were subjected to histological analysis (Fig. 6A). At 4 weeks postoperatively, the surface of the repair area was smooth in all groups without calcification or thrombus formation. HE staining revealed significant cellular infiltration in the repair area with formation of fibrous capsules in the PSP group, PSP + USCs(N) group, and PSP + USCs(H) group, while fewer cells had grown into the bovine pericardium. The materials in the bovine pericardium group, PSP group, and PSP + USCs(N) group have all maintained their structural integrity, while the scaffold materials in the PSP + USCs(H) group had maintained their structural continuity despite of partial degradation. At 8 weeks postoperatively, most of the materials in the PSP + USCs(H) group had degraded and were replaced by native-like tissues. By contrast, in the PSP and PSP + USCs(N) groups, the materials were partially degraded and gradually fused with adjacent normal tissues. At 12 weeks postoperatively, most of the materials in the PSP and PSP + USCs(N) groups had degraded and the area was mostly replaced by new tissue. The bovine pericardium had remained undegraded and was infiltrated with only a few histiocytes. Above results suggested that the PSP is more suitable for ROVT owing to its better properties for cell infiltration, biodegradation, and tissue integration. The SPS + USCs(H) bioactive patch group had the best repair effect, which was in keeping with the MRI results.

To evaluate the toxicity of the patches, lungs, liver, and kidneys of each group of animals were collected 12 weeks postoperatively. As

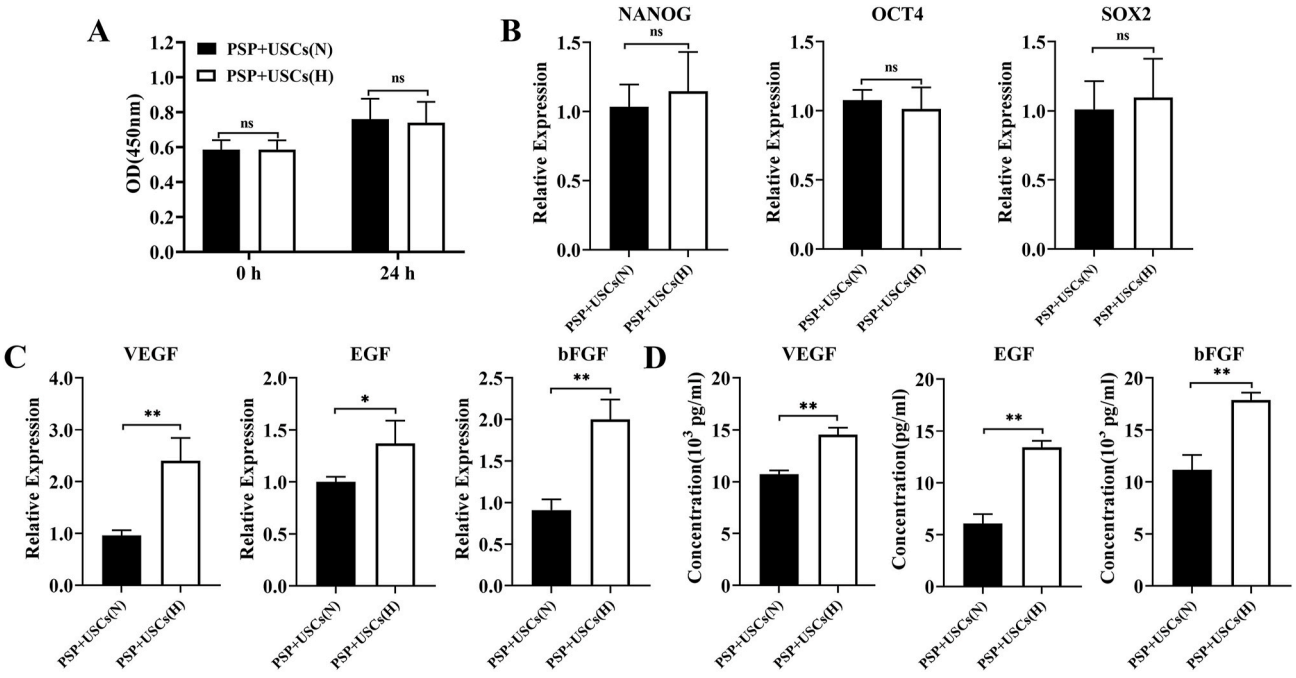

Fig. 4. Expression and secretion of angiogenic-associated cytokines in the PSP + USCs composites. (A, B) The proliferation activity and stemness gene expression of the USCs after 24 h culture under hypoxic and normal conditions. (C) Expression of angiogenic-associated cytokines in the PSP + USCs composites under hypoxic and normal conditions; (D) Cytokines secretion of the PSP + USCs composites under hypoxic and normal conditions as assessed by ELISA. Data are represented by mean ± SD. $^*P < 0.05$, $^{**}P < 0.01$, *t*-test.

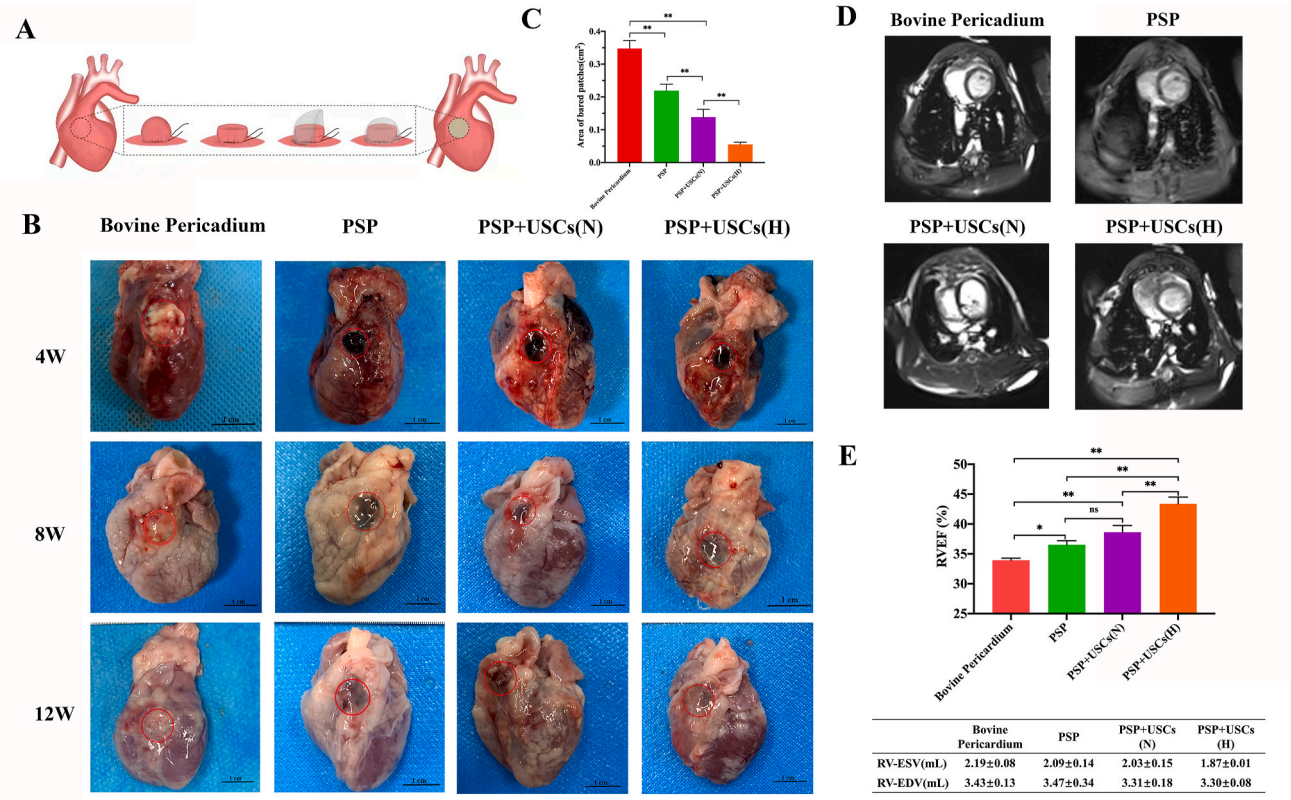

	Bovine Pericardium	PSP	PSP+USCs (N)	PSP+USCs (H)
RV-ESV(mL)	2.19±0.08	2.09±0.14	2.03±0.15	1.87±0.01
RV-EDV(mL)	3.43±0.13	3.47±0.34	3.31±0.18	3.30±0.08

Fig. 5. Establishment of a rabbit model for right ventricle wall replacement (A) Surgical procedures for the RVOT reconstruction. (B) Digital images of the patched defects at 4, 8, and 12 weeks post-operatively. Red circles have marked the region of defects. Scale bar = 1 cm. (C) Quantitative analysis of the bared patches area 8 weeks after the surgery. Data are represented as mean ± SD. *$P < 0.05$, **$P < 0.01$, one-way ANOVA. (D) Representative MRI images of the heart ventricle 12 weeks after the surgery. (E) Right ventricular end-diastolic volumes (RV-EDV), end-systole volumes (RV-ESV) and right ventricular ejection fraction (RVEF) of the patched hearts 12 weeks after the surgery. Data are represented by mean ± SD. *$P < 0.05$, **$P < 0.01$, one-way ANOVA. (For interpretation of the references to color in this figure legend, the reader is referred to the Web version of this article.)

noted, the organs from each group have retained normal color and had no necrotic foci or thrombosis (Fig. S6), which suggested that the degradation product of the PSP did not cause significant toxic damage to such organs.

Fibrosis is a major challenge to functional tissue regeneration. Scar fibrosis, mainly consisted of type I collagen, is formed by accumulation of myofibroblasts and excessive deposition of ECM proteins and can lead to increased stiffness, pathological signaling, and impaired electromechanical coupling of cardiomyocytes [38]. In this study, the extent of fibrosis was evaluated by Masson trichrome staining. As shown in Fig. 6B and C, highly collagenous areas were observed in all samples 4 weeks after the implantation. Particularly, the bovine pericardium group has developed a significantly greater collagenous area at 4, 8, and 12 weeks compared with other groups ($P < 0.05$). However, the results of HE staining showed that only a small number of cells have grown into the bovine pericardium, making it difficult to deposit more collagen fibers. We speculated that these may not be collagen fibers deposited by the fibrosis, but collagens from the bovine pericardium itself. Quantitative analysis of sectioned tissue images demonstrated that the fibrotic area of the PSP + USCs (H) group was significantly smaller compared with those of the PSP + USCs (N) and the PSP groups at 8 and 12 weeks postoperatively ($P < 0.05$), while no significant difference was detected in between the PSP + USCs (N) group and the PSP group ($P > 0.05$), suggesting that hypoxia-pretreatment could suppress fibrosis. This may be due to the fact that hypoxic preconditioning can enhance the viability of the USCs [39], which in turn may improve the condition for regeneration and facilitate infiltration of the cells into the engineered patches, resulting in an active constructive remodeling process.

3.6. Promotion of revascularization and muscularization by hypoxia-pretreated bioactive patches

Immunofluorescence staining of α-SMA in the patched area at 4, 8, and 12 weeks postoperatively was used as a measure of muscularization. As shown in Fig. 7A, the level of α-SMA expression was the highest in the PSP + USCs (H) group, whist fewer α-SMA -positive cells were noted in the patch area of the bovine pericardium group. The level of α-SMA expression in the PSP + USCs (N) group was greater than that of the PSP group (Fig. 7D). The number of blood vessels was counted by immunofluorescence staining with CD31 in the patched area at 4, 8, and 12 weeks postoperatively (Fig. 7B). A small number of new blood vessels have appeared at the site of patch in the PSP + USCs (H) group at 4 weeks postoperatively, while almost no neovascularization was noted in the other groups. At 8 and 12 weeks postoperatively, the number of blood vessels in the PSP + USCs (H) group was significantly increased ($P < 0.01$) and was much greater than those of other groups. Furthermore, more neovascularization was detected in the PSP + USCs (N) group at 8 and 12 weeks postoperatively compared with the PSP group (Fig. 7E). No significant revascularization was noted in the bovine pericardial group. Immunofluorescence staining has indicated that hypoxia-pretreated bioactive patches have remarkably promoted the revascularization and muscularization of the RVOT.

3.7. Suppression of calcification by the PSP patches

For cardiovascular tissue engineering, the resistance to calcification of the patch is also an important factor which may affect the outcome of long-term repair. An important measure for the anti-calcification

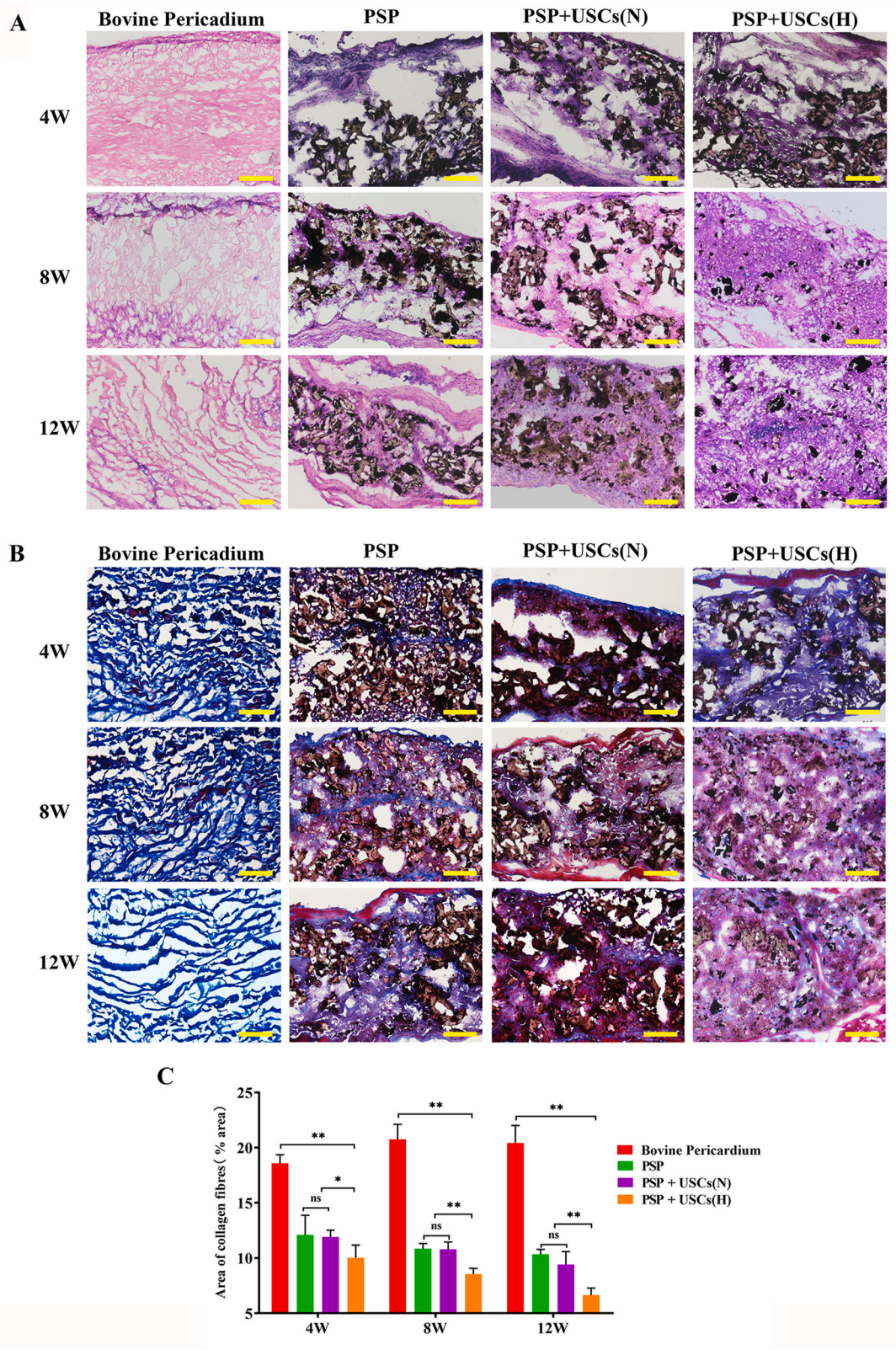

Fig. 6. Histological analysis of the patched cardiac tissue areas. (A) H&E and (B) Masson staining revealed cardiac structures in the bovine pericardium, PSP, PSP + USCs(H), and PSP + USCs(N) groups. Scale bar = 200 μm. (C) Quantitative analysis of the fibrosis area. Data are represented as mean ± SD. *$P < 0.05$, **$P < 0.01$, one-way ANOVA.

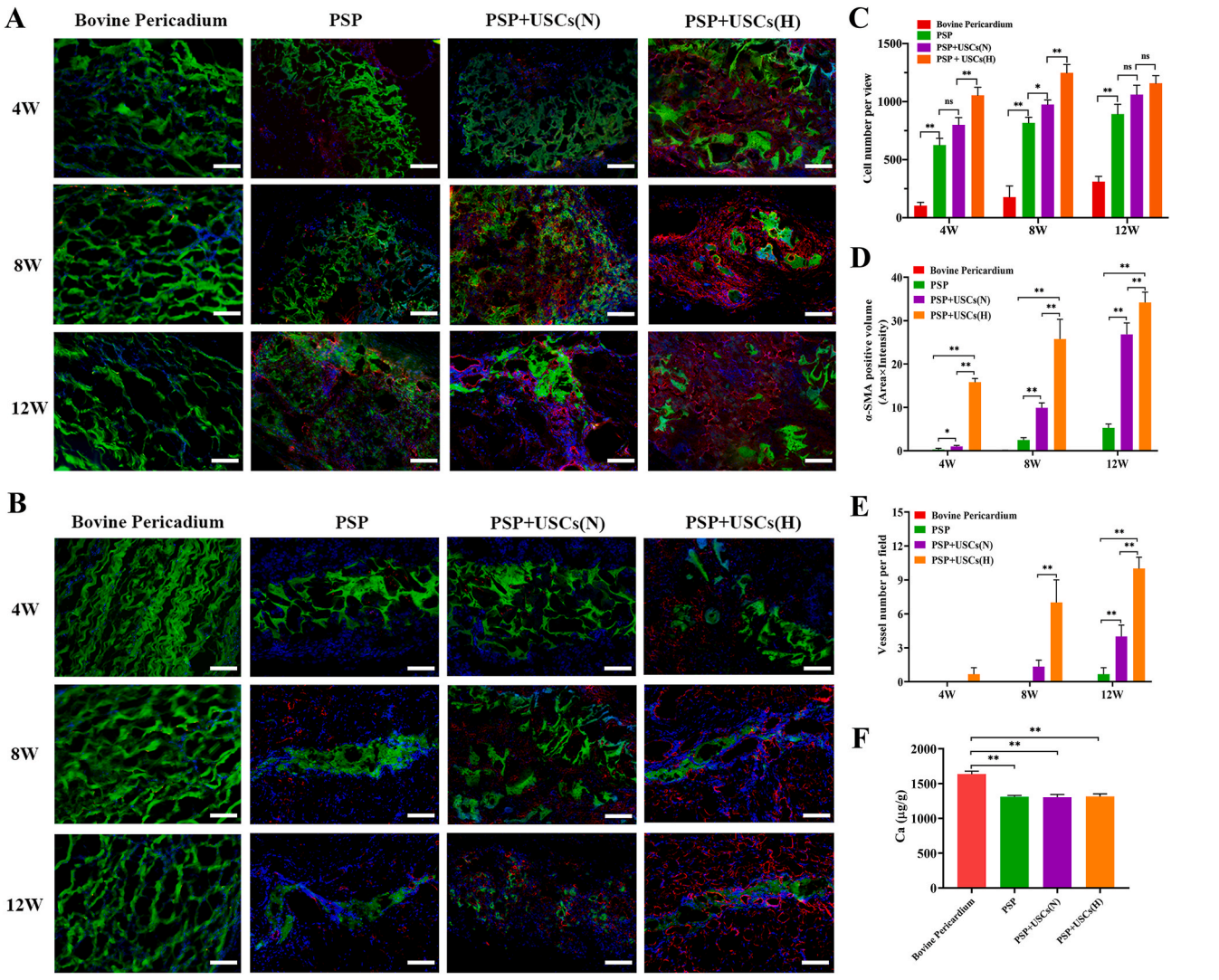

Fig. 7. Muscularization and vascularization at 4, 8, and 12 weeks postoperatively. (A) Immunohistochemistry staining of α-SMA (red) indicates muscularization at the center of defect. Scale bar = 100 μm. (B) CD31 (red) staining indicated blood vessels. Scale bar = 100 μm. (C) Quantification of cells within the patches by DAPI staining. (D, E) Quantification of α-SMA expression and number of blood vessels at various timepoints. (F) Calcium content of the center region. Data are represented by mean ± SD. $^{*}P < 0.05$, $^{**}P < 0.01$, one-way ANOVA. (For interpretation of the references to color in this figure legend, the reader is referred to the Web version of this article.)

properties of the material is the calcium content of the postoperative specimen as determined by atomic flame absorption spectroscopy [40]. To treat bovine pericardium and autologous pericardium with glutaraldehyde can lead to changes in the collagen fibers and increased deposition of calcium ions on the material [41]. In this study, the calcium content of the PSP, PSP + USCs (N), and PSP + USCs(H) groups were significantly lower than that of the bovine pericardium group, indicating that the PSP complex has a good anti-calcification property (Fig. 7F), though its long-term effect will require further investigation.

4. Discussion

Congenital heart disease affects approximately 1% of newborns and its treatment may involve surgical repair of the defect with a cardiac patch. Currently used patches have shortcomings such as non-degradation, non-conductivity, and tendency for calcification. A new cardiac patch is therefore in great demand. However, researches on heart regeneration have so far mostly focused on the treatment of myocardial infarction, with only a few focused on the development of cardiac patches to reduce the surgical complications. In this study, we have developed a novel patch with properties to suit the reconstruction of ventricular outflow tract.

An ideal cardiac patch should have good biocompatibility, biodegradability, adequate tensile strength, and conductivity similar to that of native heart tissue. Among these, mechanical property is the foremost consideration in cardiac patch design [42]. As the center of the circulatory system, the heart possesses a high elasticity modulus ranging from 22 kPa at the end of the diastole up to 500 kPa at the end of the systole [19,43]. In our previous study, we have developed a PU/SIS composite with high bioactivity, resilience, and elastic modulus suitable for cardiac tissue engineering [20]. Hence, we have tried to endow the PU/SIS with conductivity by combining the polymers to obtain a conductive scaffold material for cardiac repair.

For its sound biocompatibility, high conductivity, easy synthesis, and environmental stability, PPy is one of the most studied conductive polymers for biomedical applications [26,44]. PPy-contained conductive composites have been extensively studied for the treatment of myocardial infarction and have proven to be effective for boosting the transmission of electrophysiological signals and can remarkably improve the function and revascularization of the infarct myocardium

[18,28,29]. In this study, chemical oxidation polymerization of the PPy was used to modify the PU/SIS substrate surface *in situ*, and three PSP complexes in various proportions were obtained. By taking mechanical property, surface morphology and electrical conductivity into consideration, 0.2 mol/L pyrrole solution was selected to prepare the PSP composites (Fig. S2). As shown in Fig. 2, polymerization of the PPy has altered the surface properties of the PU/SIS but not its mechanical properties. Furthermore, the electrical conductivity was significantly increased by the polymerization of pyrrole.

Degradation is another important property for cardiac patches, as non-degradable patches cannot grow with the patient's heart. Furthermore, non-biodegradable patches may induce an inflammatory reaction to foreign body, resulting in lack of elasticity as the material becomes encapsulated in fibrous scar-like tissue, which may prevent the recovery of local tissue function [3]. As shown in Fig. 3D, the PSP could degrade slowly *in vivo*, while bovine pericardium was completely undegraded. A similar phenomenon was also observed with immunofluorescence staining, since both bovine pericardium and PSP composites have autofluorescence at 488 nm (Fig. 3E). In addition to its chemical structure, cell invasion is another factor which may affect the degradation of the material. Biological enzymes such as esterases or hydrolases secreted by cells play an important role in the biodegradation of materials. In this study, PSP composites showed a better cellular invasion, while bovine pericardium was almost devoid of cellular invasion (Fig. 7C). Analysis of degradation and cellular invasion suggested that PSP is more suitable than bovine pericardium for the repair of full-layer cardiac defects. The better biocompatibility and slower degradation of PSP might facilitate functional reconstruction of the heart defect and reduce secondary surgery. Through the RVOT model, we have demonstrated that PSP could significantly improve the cardiac function compared with the commercially made bovine pericardium, and that vascularization and muscularization of PSP composites were superior to those of the bovine pericardium (Figs. 5B and 6). This has suggested the potential of the PSP composites to be used for the make of cardiac patches. However, the area of fibrosis in the PSP group remained large, which may affect the recovery of cardiac function (Fig. 6C). Coincidentally, a recent study by Jacot et al. showed that, compared with fixed bovine pericardium, the multi-layered patch could improve the RVEF in a RVOT reconstruction model, but also induce significant fibrosis in the right ventricle wall as well as relatively poor vascularization, both of which are major obstacles for cardiac tissue engineering [36].

mscs are regarded as a class of adult stem cells for which great progress has been made in both basic and clinical research, in particular treatment of myocardial infarction. Studies have shown that the MSCs could induce an early shift from the inflammation phase to the reparative phase, reduce apoptosis and fibrosis, and enhance angiogenesis and cardiac function recovery in animal model for infarction.[45, 46] Céline Mias et al. have demonstrated that MSC exosomes could suppress fibrosis in the infarcted area of the heart by inhibiting proliferation of fibroblasts, promoting synthesis of metalloproteinases, and stimulating angiogenesis.[47] In this study, we have tried to construct PSP + USCs bioactive patches to promote right ventricle wall reconstruction and reduce fibrosis. As we have demonstrated in our previous study, hypoxia-pretreatment could enhance the paracrine function of the USCs, promote angiogenesis, and suppress fibrosis at the early stages of wound healing.[33] Therefore, we have pretreated the PSP + USCs bioactive patches with hypoxic conditions to explore the feasibility of using the USCs and hypoxia-pretreatment to promote angiogenesis and suppress fibrosis during the reconstruction of ventricular outflow tract. Our results showed that hypoxia preconditioning could promote the secretion of a large number of angiogenesis-related factors by the USCs, but did not affect its stemness gene expression and viability (Fig. 4). In the ROVT model, the normoxic pretreated PSP + USCs could improve the cardiac function through promotion of angiogenesis, but did not significantly suppress the fibrosis. The hypoxia-preconditioned PSP + USCs showed a profound effect on promoting angiogenesis and inhibiting fibrosis. We speculate that these may be due to the fact that hypoxic preconditioning has improved the survival and engraftment of the transplanted cells.[39] Cells in patches were less likely to survive after the transplantation due to low oxygen and nutrition supply in the defective area, [48] while hypoxia-pretreatment could enhance the survival and paracrine effect of the transplanted cells thereby improving the local regenerative microenvironment.[33, 39] As shown in Fig. 4, the paracrine function of the USCs was enhanced with the hypoxic conditioning. Cytokines such as VEGF, bFGF and EGF secreted by the USCs are capable of promoting cell proliferation and migration and inhibit apoptosis, [49, 50] which can promote cell infiltration into the local tissue. At 4 weeks postoperatively, more cells have grown into the centre of the PSP + USCs (H) patches compared with the other groups (Fig. 7C). Additionally, the rate of graft degradation was significantly higher in the hypoxic pretreatment group compared with other groups (Figs. 6 and 7), which may also be an important reason why the area of fibrosis was significantly smaller in the hypoxic pretreatment group. The graft is regarded as a xenobiotic by the immune system, which often triggers an inflammatory response. It is widely accepted that inflammation is associated with pathological fibrosis, and that the MSCs also have immunomodulatory functions. Therefore, the hypoxic pretreatment might have reduced the inflammatory response in the graft area by promoting graft degradation and immunomodulatory function of the USCs, thereby reducing the area of fibrosis.

As MSCs derived from the human body, the USCs may induce immune rejection after being transplanted into an immunocompetent xenogeneic body. However, the reduced expression of major histocompatibility complexes and associated proteins on the cell surface also suggested an immunological privilege for the MSCs. Many studies have shown that the MSCs can affect both the innate and adaptive immunities by inhibiting the proliferation and expression of chemotactic ligands and co-stimulatory molecules of B-cells [51], inhibiting the differentiation of Th1 and Th17 subsets of helper T cells whilst promoting the generation of regulatory T cells [52,53], inducing dendritic cells to acquire a tolerogenic phenotype through the IL-6-mediated upregulation of SOCS1 [54], and switching macrophages from the pro-inflammatory type 1 to an anti-inflammatory type 2 phenotype [55]. The MSCs have also shown promising results in treating autoimmune diseases such as systemic lupus erythematosus, rheumatoid arthritis and graft-versus-host disease [56,57]. Human MSCs have also attained good effect in treating myocardial infarction in rats. Kocher et al. [58] have found that intravenous injection of human bone marrow donor cells to rats with myocardium infarction could attenuate cardiomyocyte apoptosis and left ventricular remodeling. In another study, human mesenchymal stromal cells have improved left ventricular function, perfusion, and remodeling in a porcine model for chronic myocardial ischemia [59]. Of note, significant immune rejection was detected in none of such studies.

The cardiac outflow tract is mainly consisted of cardiomyocytes, smooth muscle cells and fibroblasts. It is well known that myocardial regeneration is difficult in adult animals [60]. Mature cardiomyocytes have a poor proliferation and migration capacity [61,62]. By immunofluorescence staining, no troponin-I positive cardiomyocyte was observed in the central area of regeneration (Fig. S7), and no significant cardiomyocyte migration was detected at the edge of the patches (Fig. S8). On the other hand, a large number of fibroblasts and smooth muscle cells were found in the cardiac tissue. Cardiac outflow tract repair and regeneration might depend mainly on fibroblasts and smooth muscle cells. The nascent cardiac tissue in the PSP group is mainly consisted of fibroblasts. As confirmed by Masson staining, more smooth muscle cells have been regenerated in the PSP + USCs(H) group, which is evidenced by more collagen fibers secreted by the fibroblasts in the PSP group and more muscle fibers presented in the smooth muscle cells in the PSP + USCs(H) group. A previous study has shown that hypoxia has a marked impact on smooth muscle regeneration. Hypoxia can promote the differentiation of the MSCs into smooth muscle cells by

regulating the Mettl3 and paracrine factors [63,64]. Moreover, hypoxia can suppress myofibroblast differentiation by altering the activity of RhoA [65]. Compared with fibroblasts, smooth muscle cells may contribute more to the maintenance of cardiac functions. A study by Harada et al. has demonstrated that, compared with fibroblasts, smooth muscle cell sheets could suppress the process of cardiac remodeling and improve the cardiac function in a myocardial infarction model [66]. In the present study, better cardiac function was also noted in the PSP + USCs(H) group, which was in keeping with previous reports.

In this study, we have developed a novel cardiac patch and explored its feasibility for the reconstruction of RVOT. Compared with commercially made bovine pericardium, the PSP patches have shown a greater potential for promoting cellularization, angiogenesis and muscularization. Furthermore, hypoxia-pretreated bioactive patch could significantly suppress fibrosis whilst promote vascularization and muscularization, resulting in a better right heart function. Our findings suggested that the PSP patches combined with hypoxic pretreated USCs may provide a strategy for the treatment of congenital heart disease. However, we have only focused on fibrosis in RVOT reconstruction and the efficiency of electrical coupling of the PSP patch with myocardial wall. Its effect on the cardiac conductive network has not been assessed. For the next step, we will focus on the safety and efficacy of the PSP patch and its effect on cell biology and electrophysiology for the reconstruction of ventricular outflow tract under electrical stimulation.

5. Conclusion

In this study, we have developed a novel cardiac patch with mechanical and electrical properties similar to those of natural myocardial tissue by compounding pyrrole with the PU/SIS. The PSP patch has shown to degrade slowly during the process of tissue reconstruction, which may reduce the need for secondary surgery in neonatal patients. Furthermore, through a RVOT reconstruction model, we have illustrated that the PSP + USCs bioactive patches could significantly reduce the fibrotic area and enhance cardiac function after a hypoxic pretreatment. Above results have demonstrated the potential of the PSP patch for the treatment of congenital heart disease as a promising candidate.

CRediT authorship contribution statement

Long-Mei Zhao: Conceptualization, Methodology, Writing of the Original Draft. **Long Wang:** Conceptualization, Methodology, Experiments, Data analysis. **Wen-Qian Zhang:** Data analysis. **Rui Wang:** Chemical experiments. **Xiu-Zhen Zhang:** Methodology, and Experiment. **Xiong-Xin Lei:** Preparation of the biomaterials. **Yan Liang:** Microscopy. **Yu-Ting Song:** Molecular experiment. **Qing-Yi Zhang:** Molecular experiment. **Ke Lin:** Conceptualization, Animal experiment. **Hui-Qi Xie:** Conceptualization, Study Design, Finalizing of the study.

Declaration of competing interest

The authors declare that they have no known competing financial interests or personal relationships that could have appeared to influence the work reported in this paper.

Acknowledgments

This work was supported by the National Key R&D Program of China (Grant No. 2017YFC1104702), National Natural Science Foundation of China (Grant No.31771065), and the 1.3.5 Project for Disciplines of Excellence, West China Hospital, Sichuan University (Grant No. ZYJC18002).

Appendix A. Supplementary data

Supplementary data to this article can be found online at https://doi.org/10.1016/j.bioactmat.2021.11.021.

References

[1] S.S. Virani, A. Alonso, E.J. Benjamin, M.S. Bittencourt, C.W. Callaway, A.P. Carson, et al., Heart disease and stroke statistics-2020 update: a report from the American heart association, Circulation 141 (9) (2020) e139–e596, https://doi.org/10.1161/CIR.0000000000000757.

[2] D. van der Linde, E.E. Konings, M.A. Slager, M. Witsenburg, W.A. Helbing, J. J. Takkenberg, et al., Birth prevalence of congenital heart disease worldwide: a systematic review and meta-analysis, J. Am. Coll. Cardiol. 58 (21) (2011) 2241–2247, https://doi.org/10.1016/j.jacc.2011.08.025.

[3] A. Mantakaki, A.O.J. Fakoya, F. Sharifpanah, Recent advances and challenges on application of tissue engineering for treatment of congenital heart disease, PeerJ 6 (2018), e5805, https://doi.org/10.7717/peerj.5805.

[4] D. Chou, A. Tulloch, D.V. Cossman, J.L. Cohen, R. Rao, G. Barmparas, et al., The influence of collagen impregnation of a knitted dacron patch used in carotid endarterectomy, Ann. Vasc. Surg. 39 (2017) 209–215, https://doi.org/10.1016/j.avsg.2016.08.011.

[5] G. Penford, D. Quandt, C. Mehta, V. Bhole, R. Dhillon, A. Seale, et al., Stenting and overdilating small Gore-Tex vascular grafts in complex congenital heart disease, Cathet. Cardiovasc. Interv. 91 (1) (2018) 71–80, https://doi.org/10.1002/ccd.27310.

[6] J.S. Gammie, K. Bartus, A. Gackowski, M.N. D'Ambra, P. Szymanski, A. Bilewska, et al., Beating-heart mitral valve repair using a novel ePTFE cordal implantation device: a prospective trial, J. Am. Coll. Cardiol. 71 (1) (2018) 25–36, https://doi.org/10.1016/j.jacc.2017.10.062.

[7] D. Bell, S. Prabhu, K. Betts, R. Justo, P. Venugopal, T.R. Karl, et al., Durability of tissue-engineered bovine pericardium (CardioCel®) for a minimum of 24 months when used for the repair of congenital heart defects, Interact. Cardiovasc. Thorac. Surg. 28 (2) (2018) 284–290, https://doi.org/10.1093/icvts/ivy246.

[8] R. Guidoin, T.M. Bes, T.F. Cianciulli, J. Klein, B. Li, R. Gauvin, et al., Cuspal dehiscence at a post and along the stent cloth in a bovine pericardium heart valve implanted for seven years, J. Long Term Eff. Med. Implants 22 (2) (2012) 95–111, https://doi.org/10.1615/jlongtermeffmedimplants.v22.i2.10.

[9] J. Mao, Y. Wang, E. Philippe, T. Cianciulli, I. Vesely, D. How, et al., Microstructural alterations owing to handling of bovine pericardium to manufacture bioprosthetic heart valves: a potential risk for cusp dehiscence, Morphologie 101 (333) (2017) 77–87, https://doi.org/10.1016/j.morpho.2017.03.003.

[10] S. Taguchi, T. Kitamura, S. Matsukuma, T. Odate, T. Ariyoshi, M. Hamawaki, et al., A case of recurrent constrictive pericarditis induced by pericardial substitution with an expanded polytetrafluoroethylene membrane, Gen Thorac Cardiovasc Surg 68 (12) (2020) 1479–1482, https://doi.org/10.1007/s11748-020-01303-8.

[11] A.D. Peivandi, M. Seiler, K.M. Mueller, S. Martens, E. Malec, B. Asfour, et al., Elastica degeneration and intimal hyperplasia lead to Contegra(R) conduit failure, Eur. J. Cardio. Thorac. Surg. 56 (6) (2019) 1154–1161, https://doi.org/10.1093/ejcts/ezz199.

[12] P. Engelfriet, E. Boersma, E. Oechslin, J. Tijssen, M.A. Gatzoulis, U. Thilén, et al., The spectrum of adult congenital heart disease in Europe: morbidity and mortality in a 5 year follow-up period, Eur. Heart J. 26 (21) (2005) 2325–2333, https://doi.org/10.1093/eurheartj/ehi396.

[13] C.J. Knott-Craig, R.C. Elkins, M.M. Lane, J. Holz, C. McCue, K.E. Ward, A 26-year experience with surgical management of tetralogy of Fallot: risk analysis for mortality or late reintervention, Ann. Thorac. Surg. 66 (2) (1998) 506–511, https://doi.org/10.1016/s0003-4975(98)00493-7.

[14] J. Zhou, X. Yang, W. Liu, C. Wang, Y. Shen, F. Zhang, et al., Injectable OPF/graphene oxide hydrogels provide mechanical support and enhance cell electrical signaling after implantation into myocardial infarct, Theranostics 8 (12) (2018) 3317–3330, https://doi.org/10.7150/thno.25504.

[15] J. Rodness, A. Mihic, Y. Miyagi, J. Wu, R.D. Weisel, R.K. Li, VEGF-loaded microsphere patch for local protein delivery to the ischemic heart, Acta Biomater. 45 (2016) 169–181, https://doi.org/10.1016/j.actbio.2016.09.009.

[16] C. Patra, S. Talukdar, T. Novoyatleva, S.R. Velagala, C. Muehlfeld, B. Kundu, et al., Silk protein fibroin from Antheraea mylitta for cardiac tissue engineering, Biomaterials 33 (9) (2012) 2673–2680, https://doi.org/10.1016/j.biomaterials.2011.12.036.

[17] T.H. Qazi, R. Rai, D. Dippold, J.E. Roether, D.W. Schubert, E. Rosellini, et al., Development and characterization of novel electrically conductive PANI-PGS composites for cardiac tissue engineering applications, Acta Biomater. 10 (6) (2014) 2434–2445, https://doi.org/10.1016/j.actbio.2014.02.023.

[18] J.H. Tsui, N.A. Ostrovsky-Snider, D.M.P. Yama, J.D. Donohue, J.S. Choi, R. Chavanachat, et al., Conductive silk-polypyrrole composite scaffolds with bioinspired nanotopographic cues for cardiac tissue engineering, J. Mater. Chem. B 6 (44) (2018) 7185–7196, https://doi.org/10.1039/C8TB01116H.

[19] Y.-K. Wu, J. Yu, The role of tissue engineering in cellular therapies for myocardial infarction: a review, J. Mater. Chem. B 3 (31) (2015) 6401–6410, https://doi.org/10.1039/c5tb00739a.

[20] L. Da, M. Gong, A. Chen, Y. Zhang, Y. Huang, Z. Guo, et al., Composite elastomeric polyurethane scaffolds incorporating small intestinal submucosa for soft tissue engineering, Acta Biomater. 59 (2017) 45–57, https://doi.org/10.1016/j.actbio.2017.05.041.

[21] S. Kim, L.K. Jang, M. Jang, S. Lee, J.G. Hardy, J.Y. Lee, Electrically conductive polydopamine-polypyrrole as high performance biomaterials for cell stimulation in vitro and electrical signal recording in vivo, ACS Appl. Mater. Interfaces 10 (39) (2018) 33032–33042, https://doi.org/10.1021/acsami.8b11546.

[22] P. Humpolicek, V. Kasparkova, J. Pachernik, J. Stejskal, P. Bober, Z. Capakova, et al., The biocompatibility of polyaniline and polypyrrole: a comparative study of their cytotoxicity, embryotoxicity and impurity profile, Mater Sci Eng C Mater Biol Appl 91 (2018) 303–310, https://doi.org/10.1016/j.msec.2018.05.037.
[23] D.O. Sanchez Ramirez, A. Varesano, R.A. Carletto, C. Vineis, I. Perelshtein, M. Natan, et al., Antibacterial properties of polypyrrole-treated fabrics by ultrasound deposition, Mater Sci Eng C Mater Biol Appl 102 (2019) 164–170, https://doi.org/10.1016/j.msec.2019.04.016.
[24] L. Yan, B. Zhao, X. Liu, X. Li, C. Zeng, H. Shi, et al., Aligned nanofibers from polypyrrole/graphene as electrodes for regeneration of optic nerve via electrical stimulation, ACS Appl. Mater. Interfaces 8 (11) (2016) 6834–6840, https://doi.org/10.1021/acsami.5b12843.
[25] K.J. Gilmore, M. Kita, Y. Han, A. Gelmi, M.J. Higgins, S.E. Moulton, et al., Skeletal muscle cell proliferation and differentiation on polypyrrole substrates doped with extracellular matrix components, Biomaterials 30 (29) (2009) 5292–5304, https://doi.org/10.1016/j.biomaterials.2009.06.059.
[26] B. Maharjan, V.K. Kaliannagounder, S.R. Jang, G.P. Awasthi, D.P. Bhattarai, G. Choukrani, et al., In-situ polymerized polypyrrole nanoparticles immobilized poly(epsilon-caprolactone) electrospun conductive scaffolds for bone tissue engineering, Mater Sci Eng C Mater Biol Appl 114 (2020), 111056, https://doi.org/10.1016/j.msec.2020.111056.
[27] N. Zanjanizadeh Ezazi, M.A. Shahbazi, Y.V. Shatalin, E. Nadal, E. Makila, J. Salonen, et al., Conductive vancomycin-loaded mesoporous silica polypyrrole-based scaffolds for bone regeneration, Int J Pharm 536 (1) (2018) 241–250, https://doi.org/10.1016/j.ijpharm.2017.11.065.
[28] S. Liang, Y. Zhang, H. Wang, Z. Xu, J. Chen, R. Bao, et al., Paintable and rapidly bondable conductive hydrogels as therapeutic cardiac patches, Adv. Mater. 30 (23) (2018), e1704235, https://doi.org/10.1002/adma.201704235.
[29] P. Divakar, I. Caruso, K.L. Moodie, R.N. Theiler, P.J. Hoopes, U.G.K. Wegst, Design, manufacture, and in vivo testing of a tissue scaffold for permanent female sterilization by tubal occlusion, MRS Adv 3 (30) (2018) 1685–1690, https://doi.org/10.1557/adv.2018.57.
[30] D. Han, J. Yang, E. Zhang, Y. Liu, C. Boriboun, A. Qiao, et al., Analysis of mesenchymal stem cell proteomes in situ in the ischemic heart, Theranostics 10 (24) (2020) 11324–11338, https://doi.org/10.7150/thno.47893.
[31] H. Cheng, S. Chang, R. Xu, L. Chen, X. Song, J. Wu, et al., Hypoxia-challenged MSC-derived exosomes deliver miR-210 to attenuate post-infarction cardiac apoptosis, Stem Cell Res. Ther. 11 (1) (2020) 224, https://doi.org/10.1186/s13287-020-01737-0.
[32] A.J. Chen, J.K. Pi, J.G. Hu, Y.Z. Huang, H.W. Gao, S.F. Li, et al., Identification and characterization of two morphologically distinct stem cell subpopulations from human urine samples, Sci. China Life Sci. 63 (5) (2020) 712–723, https://doi.org/10.1007/s11427-018-9543-1.
[33] X.R. Zhang, Y.Z. Huang, H.W. Gao, Y.L. Jiang, J.G. Hu, J.K. Pi, et al., Hypoxic preconditioning of human urine-derived stem cell-laden small intestinal submucosa enhances wound healing potential, Stem Cell Res. Ther. 11 (1) (2020) 150, https://doi.org/10.1186/s13287-020-01662-2.
[34] K. Raziyeva, A. Smagulova, Y. Kim, S. Smagul, A. Nurkesh, A. Saparov, Preconditioned and genetically modified stem cells for myocardial infarction treatment, Int. J. Mol. Sci. 21 (19) (2020) 7301, https://doi.org/10.3390/ijms21197301.
[35] G.L. Semenza, Dynamic regulation of stem cell specification and maintenance by hypoxia-inducible factors, Mol. Aspect. Med. 47–48 (2016) 15–23, https://doi.org/10.1016/j.mam.2015.09.004.
[36] S. Pok, I.V. Stupin, C. Tsao, R.G. Pautler, Y. Gao, R.M. Nieto, et al., Full-thickness heart repair with an engineered multilayered myocardial patch in rat model, Adv Healthc Mater 6 (5) (2017), https://doi.org/10.1002/adhm.201600549.
[37] K.C. Roberts-Thomson, P.M. Kistler, P. Sanders, J.B. Morton, H.M. Haqqani, I. Stevenson, et al., Fractionated atrial electrograms during sinus rhythm: relationship to age, voltage, and conduction velocity, Heart Rhythm 6 (5) (2009) 587–591, https://doi.org/10.1016/j.hrthm.2009.02.023.
[38] K.T. Weber, Y. Sun, S.K. Bhattacharya, R.A. Ahokas, I.C. Gerling, Myofibroblast-mediated mechanisms of pathological remodelling of the heart, Nat. Rev. Cardiol. 10 (1) (2013) 15–26, https://doi.org/10.1038/nrcardio.2012.158.
[39] Z. Luo, F. Wu, E. Xue, L. Huang, P. Yan, X. Pan, et al., Hypoxia preconditioning promotes bone marrow mesenchymal stem cells survival by inducing HIF-1alpha in injured neuronal cells derived exosomes culture system, Cell Death Dis. 10 (2) (2019) 134, https://doi.org/10.1038/s41419-019-1410-y.
[40] Y. Lei, Y. Xia, Y. Wang, The tropoelastin and lysyl oxidase treatments increased the content of insoluble elastin in bioprosthetic heart valves, J. Biomater. Appl. 33 (5) (2018) 637–646, https://doi.org/10.1177/0885328218807077.
[41] C. Collatusso, J.G. Roderjan, L. de Noronha, A. Klosowski, P.H. Suss, L.C. Guarita-Souza, et al., Decellularization as a method to reduce calcification in bovine pericardium bioprosthetic valves, Interact. Cardiovasc. Thorac. Surg. 8 (2019), https://doi.org/10.1093/icvts/ivz041 ivz041.
[42] S.F. Badylak, B.N. Brown, T.W. Gilbert, K.A. Daly, A. Huber, N.J. Turner, Biologic scaffolds for constructive tissue remodeling, Biomaterials 32 (1) (2011) 316–319, https://doi.org/10.1016/j.biomaterials.2010.09.018.
[43] J. Hu, M. Tomov, J. Buikema, C. Chen, M. Mahmoudi, S. Wu, et al., Cardiovascular tissue bioprinting: physical and chemical processes, Appl. Phys. Rev. 5 (2018), 041106, https://doi.org/10.1063/1.5048807.
[44] D. Gan, L. Han, M. Wang, W. Xing, T. Xu, H. Zhang, et al., Conductive and tough hydrogels based on biopolymer molecular templates for controlling in situ formation of polypyrrole nanorods, ACS Appl. Mater. Interfaces 10 (42) (2018) 36218–36228, https://doi.org/10.1021/acsami.8b10280.
[45] L. Gao, M. Yi, M. Xing, H. Li, Y. Zhou, Q. Xu, et al., In situ activated mesenchymal stem cells (MSCs) by bioactive hydrogels for myocardial infarction treatment, J. Mater. Chem. B 8 (34) (2020) 7713–7722, https://doi.org/10.1039/d0tb01320j.
[46] J.-R. Lee, B.-W. Park, J. Kim, Y.W. Choo, H.Y. Kim, J.-K. Yoon, et al., Nanovesicles derived from iron oxide nanoparticles-incorporated mesenchymal stem cells for cardiac repair, Sci Adv 66 (18) (2020), https://doi.org/10.1126/sciadv.aaz0952 eaaz0952.
[47] C. Mias, O. Lairez, E. Trouche, J. Roncalli, D. Calise, M.H. Seguelas, et al., Mesenchymal stem cells promote matrix metalloproteinase secretion by cardiac fibroblasts and reduce cardiac ventricular fibrosis after myocardial infarction, Stem Cells (Dayton, Ohio) 27 (11) (2009) 2734–2743, https://doi.org/10.1002/stem.169.
[48] S. Lee, E. Choi, M.J. Cha, K.C. Hwang, Cell adhesion and long-term survival of transplanted mesenchymal stem cells: a prerequisite for cell therapy, Oxid Med Cell Longev 2015 (2015), 632902, https://doi.org/10.1155/2015/632902.
[49] A. Adini, H. Wu, D.T. Dao, V.H. Ko, L.J. Yu, A. Pan, et al., PR1P stabilizes VEGF and upregulates its signaling to reduce elastase-induced murine emphysema, Am. J. Respir. Cell Mol. Biol. 63 (4) (2020) 452–463, https://doi.org/10.1165/rcmb.2019-0434OC.
[50] R. Kushwaha, J. Mishra, A.P. Gupta, K. Gupta, J. Vishwakarma, N. Chattopadhyay, et al., Rosiglitazone up-regulates glial fibrillary acidic protein via HB-EGF secreted from astrocytes and neurons through PPARgamma pathway and reduces apoptosis in high-fat diet-fed mice, J. Neurochem. 149 (5) (2019) 679–698, https://doi.org/10.1111/jnc.14610.
[51] A. Corcione, F. Benvenuto, E. Ferretti, D. Giunti, V. Cappiello, F. Cazzanti, et al., Human mesenchymal stem cells modulate B-cell functions, Blood 107 (1) (2006) 367–372, https://doi.org/10.1182/blood-2005-07-2657.
[52] P. Luz-Crawford, M. Kurte, J. Bravo-Alegría, R. Contreras, E. Nova-Lamperti, G. Tejedor, et al., Mesenchymal stem cells generate a CD4+CD25+Foxp3+ regulatory T cell population during the differentiation process of Th1 and Th17 cells, Stem Cell Res. Ther. 4 (3) (2013) 65, https://doi.org/10.1186/scrt216.
[53] C. Zhou, X.R. Wu, H.S. Liu, X.H. Liu, G.H. Liu, X.B. Zheng, et al., Immunomodulatory effect of urine-derived stem cells on inflammatory bowel diseases via downregulating Th1/Th17 immune responses in a PGE2-dependent manner, J Crohns Colitis 14 (5) (2020) 654–668, https://doi.org/10.1093/ecco-jcc/jjz200.
[54] Y. Deng, S. Yi, G. Wang, J. Cheng, Y. Zhang, W. Chen, et al., Umbilical cord-derived mesenchymal stem cells instruct dendritic cells to acquire tolerogenic phenotypes through the IL-6-mediated upregulation of SOCS1, Stem Cell. Dev. 23 (17) (2014) 2080–2092, https://doi.org/10.1089/scd.2013.0559.
[55] M.H. Abumaree, M.A. Al Jumah, B. Kalionis, D. Jawdat, A. Al Khaldi, F. M. Abomaray, et al., Human placental mesenchymal stem cells (pMSCs) play a role as immune suppressive cells by shifting macrophage differentiation from inflammatory M1 to anti-inflammatory M2 macrophages, Stem Cell Rev Rep 9 (5) (2013) 620–641, https://doi.org/10.1007/s12015-013-9455-2.
[56] J.Y. Lim, K.I. Im, E.S. Lee, N. Kim, Y.S. Nam, Y.W. Jeon, et al., Enhanced immunoregulation of mesenchymal stem cells by IL-10-producing type 1 regulatory T cells in collagen-induced arthritis, Sci. Rep. 6 (2016) 26851, https://doi.org/10.1038/srep26851.
[57] R. Liu, X. Li, Z. Zhang, M. Zhou, Y. Sun, D. Su, et al., Allogeneic mesenchymal stem cells inhibited T follicular helper cell generation in rheumatoid arthritis, Sci. Rep. 5 (2015) 12777, https://doi.org/10.1038/srep12777.
[58] A.A. Kocher, M.D. Schuster, M.J. Szabolcs, S. Takuma, D. Burkhoff, J. Wang, et al., Neovascularization of ischemic myocardium by human bone-marrow-derived angioblasts prevents cardiomyocyte apoptosis, reduces remodeling and improves cardiac function, Nat. Med. 7 (4) (2001) 430–436, https://doi.org/10.1038/86498.
[59] C.B. Liu, H. Huang, P. Sun, S.Z. Ma, A.H. Liu, J. Xue, et al., Human umbilical cord-derived mesenchymal stromal cells improve left ventricular function, perfusion, and remodeling in a porcine model of chronic myocardial ischemia, Stem Cells Transl Med 5 (8) (2016) 1004–1013, https://doi.org/10.5966/sctm.2015-0298.
[60] T. Eschenhagen, R. Bolli, T. Braun, L.J. Field, B.K. Fleischmann, J. Frisen, et al., Cardiomyocyte regeneration: a consensus statement, Circulation 136 (7) (2017) 680–686, https://doi.org/10.1161/CIRCULATIONAHA.117.029343.
[61] A.S. Walravens, M. Vanhaverbeke, L. Ottaviani, H. Gillijns, S. Trenson, N. V. Driessche, et al., Molecular signature of progenitor cells isolated from young and adult human hearts, Sci. Rep. 8 (1) (2018) 9266, https://doi.org/10.1038/s41598-018-26969-2.
[62] Y. Wu, L. Zhou, H. Liu, R. Duan, H. Zhou, F. Zhang, et al., LRP6 downregulation promotes cardiomyocyte proliferation and heart regeneration, Cell Res. 31 (4) (2021) 450–462, https://doi.org/10.1038/s41422-020-00411-7.
[63] F. Wang, V. Zachar, C.P. Pennisi, T. Fink, Y. Maeda, J. Emmersen, Hypoxia enhances differentiation of adipose tissue-derived stem cells toward the smooth muscle phenotype, Int. J. Mol. Sci. 19 (2) (2018) 517, https://doi.org/10.3390/ijms19020517.
[64] J. Lin, Q. Zhu, J. Huang, R. Cai, Y. Kuang, Hypoxia promotes vascular smooth muscle cell (VSMC) differentiation of adipose-derived stem cell (ADSC) by regulating Mettl3 and paracrine factors, Stem Cell. Int. 2020 (2020), 2830565, https://doi.org/10.1155/2020/2830565.
[65] L. Leinhos, J. Peters, S. Krull, L. Helbig, M. Vogler, M. Levay, et al., Hypoxia suppresses myofibroblast differentiation by changing RhoA activity, J. Cell Sci. 132 (5) (2019) jcs223230, https://doi.org/10.1242/jcs.223230.
[66] S. Harada, Y. Nakamura, S. Shiraya, Y. Fujiwara, Y. Kishimoto, T. Onohara, et al., Smooth muscle cell sheet transplantation preserve cardiac function and minimize cardiac remodeling in a rat myocardial infarction model, J. Cardiothorac. Surg. 11 (1) (2016) 131, https://doi.org/10.1186/s13019-016-0508-x.